Surface Heat Fluxes in the Western Equatorial Pacific Ocean Estimated by Bulk Parameterization and by an Inverse Mixed Layer Model

YUN HE AND XIAO-HAI YAN

Center for Remote Sensing, Graduate College of Marine Studies, University of Delaware, Newark, Delaware

W. TIMOTHY LIU

Jet Propulsion Laboratory, California Institute of Technology, Pasadena, California

(Manuscript received 27 November 1995, in final form 28 April 1997)

ABSTRACT

Sea surface heat fluxes in the western equatorial Pacific Ocean estimated by bulk parameterization are compared with fluxes computed with a one-dimensional, level 2.5 turbulence closure inverse mixed layer model. The bulk parameterization method requires the inputs of sea surface temperature, cloud amount, wind speed, air temperature, and specific humidity. With the inverse mixed layer model, the authors estimate the surface net heat flux using surface wind stresses and sea surface temperature (SST) as input, assuming a linear variation of surface heat fluxes between two time intervals of known SST in a secant root-finding algorithm. The meteorological data time series from the Woods Hole Oceanography Institution buoy at 1°45′S, 156°E during the Tropical Ocean Global Atmosphere Coupled Ocean–Atmosphere Response Experiment intensive observation period is used as the test dataset. The inverse method generates large variations in daily mean heat flux estimation while the derived longer time-averaged net heat flux is more consistent with the bulk formula result. This can be explained by an experiment that shows that the heat flux is highly sensitive to relatively small SST errors in the input. The use of satellite data is also discussed by testing the model with a blended SST input composed of satellite-observed and mooring-measured SST.

1. Introduction

The ocean is largely forced at the surface by wind stresses (momentum flux) and heat fluxes. Since direct measurements of wind stresses and heat fluxes are difficult, bulk parameterization formulae have been used to estimate the fluxes from measurements reported routinely by volunteer ships, which include cloud fraction, sea surface temperature, wind speed, air temperature, and humidity (in the form of dry bulb temperature or dewpoint temperature). The transfer coefficients were assumed to be constant or a simple function of wind speed and determined by empirical methods. The subject of bulk parameterization has been reviewed by Smith (1988), Liu (1990), and others. In theory, the coefficients depend on reference height, sea state, atmospheric density stratifications, and other factors. Liu et al. (1979, hereafter referred to as LKB) attempted to account for these factors and took a physical approach to bulk parameterization by solving simultaneously the flux-profile relations based on similarity theory. A parameterization scheme based on the LKB method, but including more parameters and more atmospheric and oceanic physics, has been developed by Fairall et al. (1996). This scheme is tuned to the TOGA (Tropical Ocean Global Atmosphere) COARE (Coupled Ocean–Atmosphere Response Experiment) data. The results of this scheme and LKB method will be compared briefly in section 4a.

Methods of estimating the fluxes have also been developed [see Liu (1990) and Liu (1993) for a review]. The estimation of solar heating uses high-resolution data (temporally and spatially) from the geostationary satellite (e.g., Gautier et al. 1980; Bishop and Rossow 1991) and the evaporative cooling depends on SST, wind speed, and water vapor measured by polar orbiting radiometers (Liu 1984; Liu 1988). The application of satellite data to estimations of both solar heating and evaporative cooling has been demonstrated by Liu and Gautier (1990) and Liu et al. (1994). They used the data in studies of the upper-ocean heat balance. Wind stresses estimated from satellite data in forcing the ocean circulation model have also been examined (e.g., Liu et al. 1993; Chen et al. 1994a; Liu et al. 1995).

Many different procedures to calculate saturation vapor pressure, thus saturation specific humidity, have been proposed (Sargent 1980). The classic procedure is

Corresponding author address: Dr. Xiao-Hai Yan, Center for Remote Sensing, Graduate College of Marine Studies, University of Delaware, Newark, DE 19716-3501.
E-mail: xiao.yan@mvs.udel.edu

the Goff–Gratch formulation (Goff and Gratch 1946) as presented in the Smithsonian Tables. Among these different procedures are Lowe's (1977) polynomial approximation used by the LKB bulk parameterization and Buck's (1981) exponential equation used by the TOGA COARE Bulk Flux Code 2.0. All these methods are based on the Clausius–Clapeyron equation, but developed to simplify the computation.

The accuracies of all these bulk formulas are not entirely satisfactory. The differences between different bulk formulas are sometimes as high as 80 W m^{-2} (Weare 1989). A difference of 25 W m^{-2} in net heat flux can produce a 3.5°C change per year in a 50-m layer of water (Seager et al. 1988), or a 1.8°C change per year in a 100-m layer (Giese and Cayan 1993), a level of error that could be intolerable in an ocean model integration (Yan and Okubo 1992).

Miller (1981) first suggested a totally different approach using a one-dimensional oceanic mixed layer model forced by wind stresses from satellite data to estimate the surface heat fluxes. He looked for successive values of the surface net heat flux that yield a nearly exact simulation of the observed SST changes. This allows us to take advantage of all observed data with their error estimates. Gaspar et al. (1990) used real data in the area and a similar approach as that of Miller. Unlike Miller's integral mixed layer model, he used a simple eddy kinetic energy parameterization of the oceanic vertical mixing of the upper ocean. The turbulence kinetic energy is defined through a prognostic equation while the turbulent length scales are defined by a diagnostic formulation.

The western equatorial Pacific is important because of the large area of warm sea surface temperature (SST), which strongly influences the global atmospheric circulation and climate variability. Significant westerly wind bursts between generally light mean wind is associated with the onset of the El Niño–Southern Oscillation phenomenon (Lukas and Lindstrom 1991; Yan et al. 1992, 1997).

In this research, we estimate the surface net heat flux separately by the bulk formula and by an inverse mixed layer model using observed variables as input at a buoy site of the western equatorial Pacific Ocean. Horizontal heat advection is not important in this region because of the weak horizontal temperature gradient (Godfrey and Lindstrom 1989). Strong vertical salinity stratification due to heavy precipitation in the warm pool area plays an important role in the mixed layer thermodynamics (Lukas and Lindstrom 1991; Delcroix et al. 1992; Sprintall and McPhaden 1994). Thus, a one-dimensional vertical mixing model with the consideration of salinity structure is simple and reasonable to apply here. In this study, the Mellor and Yamada (1982) level 2.5 turbulence closure vertical mixing scheme is adopted. Although the model's physics lacks the effects of wind stirring and vertical penetrative convection, these could be neglected in the equatorial regions (Chen et al. 1994b). The differences between our proposed inverse mixed layer model and that of Gaspar et al. (1990) are, first, the master length scale is determined by the vertical structure of the turbulent kinetic energy, rather than diagnosticly, and second, the freshwater flux is considered in the numerical model due to the local condition in the western equatorial Pacific Ocean.

Section 2 gives a detailed description of the bulk formula and the one-dimensional, level 2.5 turbulence closure inverse mixed layer model. Section 3 is a brief introduction to the dataset tested. In section 4, results of the bulk formula and the inverse mixed layer models are compared and discussed. An experiment is performed to test the sensitivity of the simulated net heat flux to SST errors in the model input. For this inverse model, we also tested the possibility of using satellite data as model input by forcing it with a blended SST (satellite-observed SST blended with mooring-measured SST). Section 5 is a brief summary of this study.

2. Methodology

a. Bulk formula

The surface fluxes of momentum (wind stresses), freshwater, radiative, latent, and sensible heat fluxes can be estimated by the bulk formula using satellite observed and directly measured variables.

Net surface heat flux Q consists of net shortwave radiation Q_I minus net longwave radiation Q_B, latent heat flux Q_E, and sensible heat flux Q_H (Stevenson and Niiler 1983; Talley 1984):

$$Q = Q_I - Q_B - Q_E - Q_H. \tag{1}$$

Net shortwave radiation is given as (Reed 1977):

$$\begin{aligned} Q_I &= Q_S(1 - \alpha) \\ &= Q_{S0}(1 - 0.62C + 0.0019\theta)(1 - \alpha), \end{aligned} \tag{2}$$

where α is the surface albedo; here we take α to be 0.055, a typical value of the TOGA COARE region; Q_{S0} is clear-sky radiation, which is a function of latitude and time of year; C is daytime averaged cloud amount in tenths; and θ is noon solar altitude in degrees.

Lumb's (1964) formula for hourly clear-sky conditions is

$$Q_{S0} = I_{SC}s(0.61 + 0.20s), \tag{3}$$

where the coefficient I_{SC} is solar constant 1353 W m^{-2} and s is the mean of the sine of the solar altitude at the beginning and end of the hour and is calculated as follows:

solar declination

$$\delta = \frac{23.45}{\pi}\cos\left[\frac{2\pi}{365}(172 - D)\right] \tag{4}$$

sine of solar altitude

$$s = \sin\delta\sin\phi + \cos\delta\cos 2\phi\cos\omega, \tag{5}$$

where D is day of year, ϕ is latitude, and ω is hour angle (degrees), which is zero at solar noon and decreases 15° every hour.

Stevenson and Niiler's (1983) formula for net longwave radiation is

$$Q_B = [\epsilon\sigma T_S^4(0.39 - 0.05e_{10}^{1/2}) + 4\epsilon\sigma T_S^3(T_S - T_{10})] \times (1 - 0.7C), \quad (6)$$

where emissivity of sea surface $\epsilon = 0.97$, Stephen–Boltzman constant $\sigma = 5.673 \times 10^{-8}$ W m^{-2} K^{-4}, e_{10} is water vapor pressure (mb) at 10-m height, T_S is sea surface temperature in K, T_{10} is atmosphere temperature (K) at 10-m height, and C is the fraction (tenths) of the sky covered by cloud.

The turbulent heat fluxes are estimated by LKB bulk parameterization in this study. The fluxes of latent, sensible heat, and momentum are computed directly from the inputs of sea surface temperature T_S, air temperature T_a, specific humidity q, wind speed U, and the heights of measurement with variable transfer coefficients C_E, C_H, and C_D. The bulk formulas are

$$Q_E = LE = \rho_a C_E L U(q_s - q), \quad (7)$$

$$Q_H = \rho_a C_P C_H U(T_S - T_a), \quad (8)$$

and

$$\boldsymbol{\tau} = \rho_a C_D U\mathbf{U}, \quad (9)$$

where Q_E is the latent heat flux, Q_H is the sensible heat flux, and $\boldsymbol{\tau}$ is the wind stresses; E is the moisture flux, $L = 2.5008 \times 10^6 - 2.3 \times 10^3\, T_S$ J kg^{-1} is the latent heat of vaporization, T_S is sea surface temperature, ρ_a is density of the air using the ideal gas equation with a correction for the virtual equation, $\rho_a = P_a/(RT_a)$, P_a is air pressure, $R = 287.04$ J kg^{-1} K^{-1} is the atmospheric constant, T_a is air temperature, U is wind speed, q_s is saturation specific humidity, q is specific humidity, C_E is the moisture transfer coefficient, C_H is the heat transfer coefficient, $C_P = 1.0048 \times 10^3$ J Kg^{-1} °C is specific heat of air at constant pressure, C_D is the transfer coefficient of momentum or drag coefficient, and $\mathbf{U}$ is the wind velocity at observation level.

b. Inverse model

The one-dimensional, level 2.5 turbulence closure model equations for zonal velocity u, meridional velocity v, temperature T, and salinity S are

$$\frac{\partial u}{\partial t} - fv = -P_x + \frac{\partial}{\partial z}\left(K_M\frac{\partial u}{\partial z}\right) \quad (10)$$

$$\frac{\partial v}{\partial t} + fu = -P_y + \frac{\partial}{\partial z}\left(K_M\frac{\partial v}{\partial z}\right) \quad (11)$$

$$\frac{\partial T}{\partial t} = \frac{\partial}{\partial z}\left(K_H\frac{\partial T}{\partial z}\right) \quad (12)$$

$$\frac{\partial S}{\partial t} = \frac{\partial}{\partial z}\left(K_H\frac{\partial S}{\partial z}\right), \quad (13)$$

where the vertical eddy coefficients K_M and K_H are calculated using the level 2.5 turbulence closure scheme of Mellor and Yamada (1982):

$$(K_M, K_H) = (lqS_M + \nu, lqS_H + \nu); \quad (14)$$

here ν is background diffusivity, q is the square root of twice the turbulence energy and is calculated from a 1D turbulence energy equation, l is the master mixing length, which can be determined according to the vertical distribution of q,

$$l = l_0\frac{\kappa z}{\kappa z + l_0} \quad (15)$$

$$l_0 = \alpha\frac{\int_{-h}^{0}|z|q\,dz}{\int_{-h}^{0}q\,dz}, \quad (16)$$

where $\kappa = 0.4$ is the von Kármán constant and h is water depth; S_M, S_H are functions of the gradient Richardson number Ri and some experimentally determined constants A_1, B_1, A_2, B_2, C_1, where

$$\mathrm{Ri} = -\frac{g}{\rho}\frac{\partial\rho}{\partial z}\Big/\left[\left(\frac{\partial u}{\partial z}\right)^2 + \left(\frac{\partial v}{\partial z}\right)^2\right] \quad (17)$$

$$(A_1, B_1, A_2, B_2, C_1) = (0.92, 16.6, 0.74, 10.1, 0.08). \quad (18)$$

These constants can be modified to improve the model performance.

Following Chen and Rothstein (1991), we assume that the vertical distribution of zonal pressure gradient is Gaussian (Dillon et al. 1989); that is, $P_x = P_{0x}\exp(-(z/h)^2)$, where $h = 500$ m and P_{0x} is chosen so that the vertical integrated P_x balances the mean zonal wind stress. The downward solar shortwave irradiance has the form of $I(z) = 0.58\, e^{z/h_1} + 0.42\, e^{z/h_2}$, where $h_1 = 1$ m and $h_2 = 18$ m for ocean water Type IB (Paulson and Simpson 1977).

At the ocean surface,

$$\left.\begin{aligned} K_M\left(\frac{\partial u}{\partial z}, \frac{\partial v}{\partial z}\right) &= (\tau^\lambda, \tau^\phi) \quad (19)\\ K_H\left(\frac{\partial T}{\partial z}, \frac{\partial S}{\partial z}\right) &= \left(\frac{Q}{\rho C_P}, S_f S\right) \quad (20)\end{aligned}\right\} \quad \text{at } z = 0,$$

where $(\tau^\lambda, \tau^\phi)$ are the zonal and meridional components of wind stresses, and (Q, S_f) are the surface net heat and freshwater fluxes. All these fluxes are specified except Q, which is to be determined by inverse techniques.

At the model bottom, there are no fluxes of momentum, heat, and salt:

$$\frac{\partial u}{\partial z} = \frac{\partial v}{\partial z} = \frac{\partial T}{\partial z} = \frac{\partial S}{\partial z} = 0 \quad \text{at } z = -h. \quad (21)$$

We can model the upper-ocean mixed layer structure by setting the water column as being 500-m deep with a constant grid spacing of 10 m. The initial current velocity is zero; the initial temperature profile is interpolated from daily mean vertical temperature field at different depths. The initial salinity profile is derived from climatological salinity vertical structure of that month. An implicit method with a time step of 1 h is used to solve Eqs. (10)–(13). The result of implicit finite-difference scheme of the equations are solved with a tridiagonal matrix reduction technique. At each time step, eddy diffusion coefficients are recomputed through an iteration.

The inverse method estimates surface net heat flux starting from the initial state at time t_0 when all fluxes, including τ^{λ}, τ^{ϕ}, S_{ρ}, and initial Q, are known. Here initial net surface heat flux Q_0 is calculated from the bulk formula. A linear variation of surface heat fluxes between intervals of two time instants of known SST is then assumed; that is, let $Q_1 = Q_0 + \beta t$ be the surface heat fluxes during the time period between t_0 and t_1, where t_1 is the first time at which the SST is known. The secant method used to determine the linearly increasing rate of the heat flux β usually converges faster than the bisection method. Now given the first two guesses of β_1 and β_2, let $Q_1 = Q_0 + \beta_1 t$ and $Q_2 = Q_0 + \beta_2 t$, integrate the model forward from t_0 to t_1 and obtain simulated SST_1 and SST_2 respectively at time t_1. The next two guesses of β may be chosen as 1) the β that yields the smaller discrepancy of SST between β_1 and β_2, that is,

$$\beta_{1\mathrm{new}} = \beta_1 \quad \text{if } \mathrm{SST}_1 - \mathrm{SST} > \mathrm{SST}_2 - \mathrm{SST}$$
$$= \beta_2 \quad \text{otherwise; and} \qquad (22)$$

2) the intersection of the secant line connected by (β_1, $\mathrm{SST}_1 - \mathrm{SST}$) and ($\beta_2$, $\mathrm{SST}_2 - \mathrm{SST}$) with β axis, that is,

$$\beta_{2\mathrm{new}} = \beta_1 + \frac{(\mathrm{SST} - \mathrm{SST}_1)}{(\mathrm{SST}_2 - \mathrm{SST}_1)}(\beta_2 - \beta_1). \qquad (23)$$

Then integrate the model with $\beta_{1\mathrm{new}}$ and $\beta_{2\mathrm{new}}$. Repeat the above procedure until the simulated and known SST at time t_1 agree within an accepted tolerance; here we choose 0.01°C. Usually the procedure converges within five iterations. The choice of the initial heat flux value does not affect the final convergence but rather affects the number of iterations needed. Then the estimation continues by repeating the same iterative procedure between t_1 and t_2, the next time instant at which the SST is known.

3. Data sources and analysis

The integrated meteorological (IMET) buoy of Robert Weller and the Woods Hole Oceanographic Institution (WHOI) was deployed in the center of the intensive flux array (IFA) at 1°45′S, 156°E during TOGA COARE intensive observation period (IOP). The meteorological hourly time series (Weller and Anderson 1996) used in this study include: wind speed, wind stress, rainfall rate, relative humidity, barometric pressure, air temperature, sea surface temperature, net shortwave radiation, net longwave radiation, latent heat flux, and sensible heat flux. A four-day gap from 9 to 13 December 1992 was filled with hourly data from a nearby Autonomous Temperature Line Acquisition System (ATLAS) buoy at 2°S, 156°E by M. McPhaden at the National Oceanic and Atmospheric Administration (NOAA)/Pacific Marine Environmental Laboratory (PMEL). The measurement heights for wind speed, relative humidity, barometric pressure, and air temperature are 3.54 m, 2.74 m, 3.00 m, and 2.78 m, respectively. Sea surface temperature is measured at 0.45-m depth. Both net shortwave and net longwave radiations are obtained by combining observed incoming radiation and estimated outgoing radiation from the bulk formula. The latent and sensible heat fluxes in this dataset are estimated by TOGA COARE Bulk Flux Code 2.0. Hereafter, we will refer the heat fluxes (net shortwave radiation, net longwave radiation, latent heat flux, and sensible heat flux) of this dataset as ''IMET fluxes.''

Monthly International Satellite Cloud Climatology Project 2° × 2° cloud cover fields (Rossow and Schiffer 1991) are interpolated at 1°45′S, 156°E and used for obtaining net shortwave radiation from Eq. (2) and net longwave radiation from Eq. (6). It is worth noting that the temporally varying cloud fraction has a very significant effect on the surface irradiance (Lumb 1964; Chen et al. 1994a).

The net shortwave radiation is estimated from Eq. (2) with the above available cloud cover data at the WHOI buoy and compared with IMET flux. The net longwave radiation equation (6) uses sea surface temperature, air temperature, water vapor pressure, and cloud cover as input at the WHOI buoy and the results are compared with IMET flux. The wind speed, sea surface temperature, and air temperature, as well as their observation heights, are used in Eqs. (7)–(9) to estimate hourly latent heat fluxes, sensible heat fluxes, and wind stresses. Especially, the relative humidity and water vapor pressure are used to calculate the specific humidity difference for the latent heat flux estimation.

Five day averaged 2.5° × 2.5° Global Precipitation Climatology Project (GPCP) infrared-based precipitation estimates (Janowiak and Arkin 1991) from 1986 to the first 18 pentads of 1994 are used for the freshwater flux. The rain rate at 1°45′S, 156°E is obtained by linear spatial interpolation and is assumed constant in one pentad.

In this study, we also want to test the practical usage of satellite-derived SST in the inverse model. Satellite-derived SST during TOGA COARE IOP is provided by William Emery and Keith Cherkauer at University of Colorado. The raw data is collected from the advanced very high resolution radiometer (AVHRR) aboard the

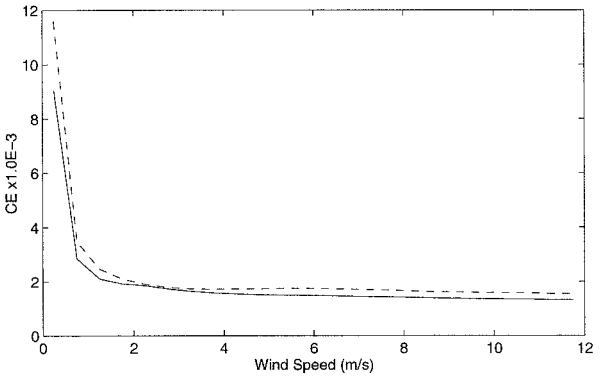

FIG. 1. Moisture transfer coefficients averaged in wind speed bins of 0.5 m s^{-1} for the WHOI buoy. Solid line: TOGA COARE Bulk Flux Code 2.0; dashed line: LKB bulk parameterization.

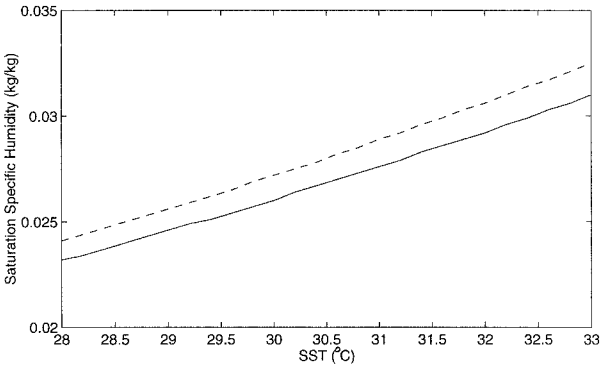

FIG. 2. Saturation specific humidity calculated by two different procedures at constant surface pressure of 1013 mb. Solid line: Buck's (1981) exponential equation used by TOGA COARE Bulk Flux Code 2.0; dashed line: Lowe's (1977) polynomial approximation used by LKB bulk parameterization.

NOAA-11, -12 near-polar, sun-synchronous orbiting satellites at the satellite ground station operated by James Cook University (Townsville, Australia).

Two NOAA satellites provide twice-daily (thermal band) coverage across the COARE area from an altitude of 840 km. The datasets we have are 1024 by 512, 16-bit images from various sea surface temperature algorithms: multichannel SST (MCSST), cross-product SST (CPSST), nighttime cross-product SST (CPSST3), and satellite skin SST (SMSST) over the region of (10°S, 10°N) by (140°E, 180°) from both *NOAA-11*, *NOAA-12* passes. Due to the lack of in situ skin SST measurements, it is difficult to say which of the algorithms produces the most accurate results (Wick et al. 1992). In this study, CPSST and CPSST3 are chosen as daytime and nighttime satellite-observed SST, respectively. Because of the large amount of cloud cover over the region, the valid data is very limited.

Since actual SST is usually higher than the satellite-observed SST with unremoved cloud cover effect, the highest SST value within a 1° by 1° region at 1°45′S, 156°E is used. If such chosen SST value is too high (higher than 31.5°C for this point), we use the value of the nearest available point instead. If this value is still too low (lower than 28°C) for this point, we assume that satellite-observed SST for this point is not good and just drop it. Daily mean satellite-observed SST is obtained by averaging all the available values from the satellite passes on that day. *NOAA-11, -12* AVHRR-derived SST is then blended with mooring-measured SST for those days without satellite data. This blended SST is then used in the inverse model.

4. Results and discussion

a. Bulk formula

Some surface latent and sensible heat fluxes are included in the WHOI buoy data. They were computed using the TOGA COARE Bulk Flux Code 2.0, as indicated in section 3. The IMET latent heat flux acquired from this dataset in the form of a transfer coefficient averaged over 0.5 m s^{-1} wind speed bins are compared with those computed using the LKB method in Fig. 1. The two sets of data agree closely with little significant difference. Figure 2 shows the saturation specific humidity calculated by two different procedures in the SST range of interest: Buck's (1981) exponential equation used by TOGA COARE Bulk Flux Code 2.0, Lowe's (1977) polynomial approximation used by LKB bulk parameterization. Surface pressure is assumed constant as 1013 mb in both cases. The mean percentage difference between these two methods is 4.3%. Although Buck's result is consistently lower than Lowe's result in this figure, it does not imply any systematic difference between two methods when a larger range of SST is considered. From the above results, we can conclude that the latent heat fluxes calculated by the TOGA COARE bulk flux code do not differ significantly from the LKB bulk formula.

Figure 3 shows the comparison of IMET and the bulk-formula-derived (a) monthly mean net shortwave radiation, (b) monthly mean net longwave radiation, (c) daily mean latent heat flux, (d) daily mean sensible heat flux, and (e) daily mean net heat flux. Since we do not have high-resolution cloud cover data, net shortwave radiation and longwave radiation are compared monthly instead of daily. The correlation coefficients between the two lines in Figs. 3a and 3b are 0.63 and 0.45, respectively. The mean differences for net shortwave radiation and net longwave radiation are 1.99 and 4.36 W m^{-2}, respectively. From Fig. 3b, we can see that bulk-formula-derived net longwave radiation is consistently lower than IMET values. This may be caused by the usage of barotropic pressure measured at 3.00 m and air temperature at 2.78 m instead of values at 10-m height in the bulk formula. IMET net shortwave and longwave radiation, instead of the bulk formula fluxes that were estimated with monthly cloud cover, are used for both net heat fluxes compared in Fig. 3e to show

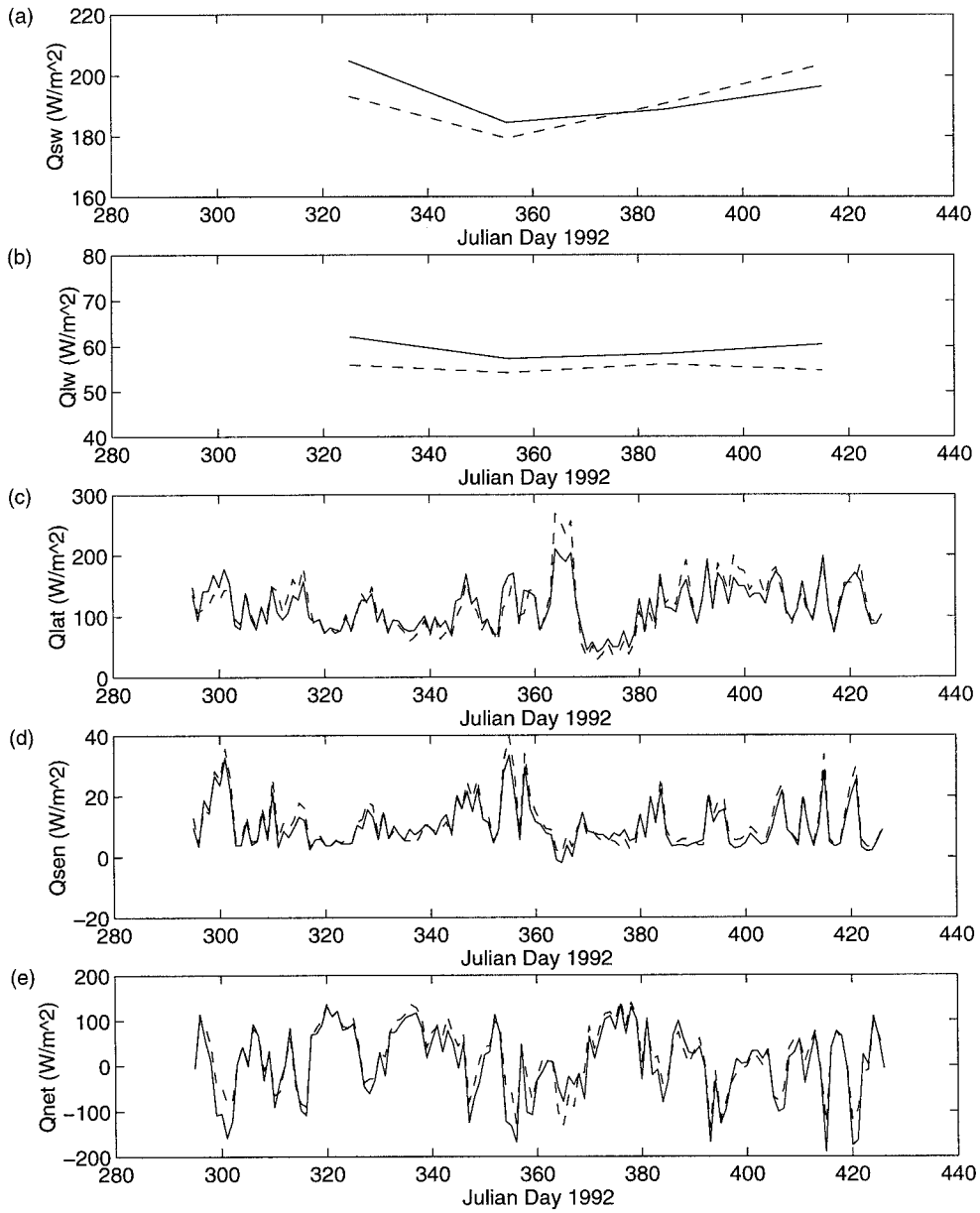

FIG. 3. IMET (solid) and the bulk-formula-derived (dashed) (a) monthly mean net shortwave radiation, (b) monthly mean net longwave radiation, (c) daily mean latent heat flux, (d) daily mean sensible heat flux, and (e) daily mean net heat flux for the WHOI buoy.

how accurately net heat flux could be estimated when radiation data is available. The correlation coefficients between the two lines in Figures 3c, 3d, and 3e are 0.93, 0.97, and 0.95 respectively.

Satellite data is a major data source covering large areas. We can use satellite observed variables in the bulk formula. Surface humidity, wind speed, sea surface temperature, relative humidity (Liu and Niiler 1984; Liu 1988) and cloud cover (Gautier et al. 1980; Gautier and Frouin 1985) can all be derived from satellite measurements. Twice-daily satellite data coverage is frequent enough for producing the heat fluxes averaged over several days or longer.

b. Inverse model

Figure 4 gives the daily mean net heat fluxes estimated by the bulk formula and those derived by the inverse model for the WHOI buoy. The inverse-model-derived net heat flux has a larger variation than the bulk formula estimation, a result also shown in the study of Gaspar et al. (1990). The correlation coefficient between

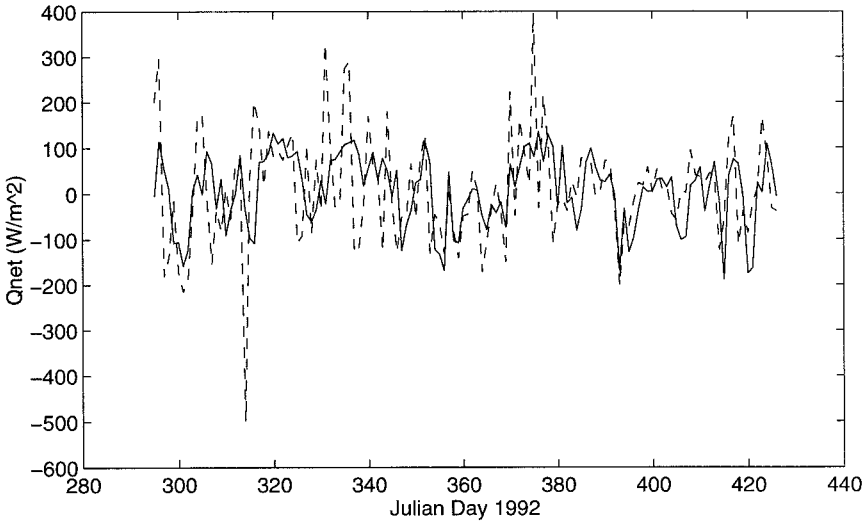

FIG. 4. Daily mean net heat fluxes estimated by the bulk formula and those derived by the inverse model (dashed) for the WHOI buoy.

the two lines is 0.39. But the mean net heat fluxes for both methods are 7.4 and 9.8 W m^{-2}, the difference is small.

Large and Pond (1982) pointed out that the bulk method is not suitable for estimating instantaneous fluxes, but rather mean values over a few days, the period needed to average out the effects of the nonparameterized processes. So, if we look at a longer time average of net heat fluxes for the WHOI buoy (Fig. 5), we can see that the inverse model estimates more accurately the longer time-averaged net heat flux. The correlation coefficients for 5-day, 15-day, and 30-day averaged net heat fluxes between the bulk formula estimates and the inverse model results are 0.78, 0.95, and 0.84, respectively. The mean differences for 5-day, 15-day, and 30-day averaged net heat fluxes are 3.4, 0.05, and 0.05

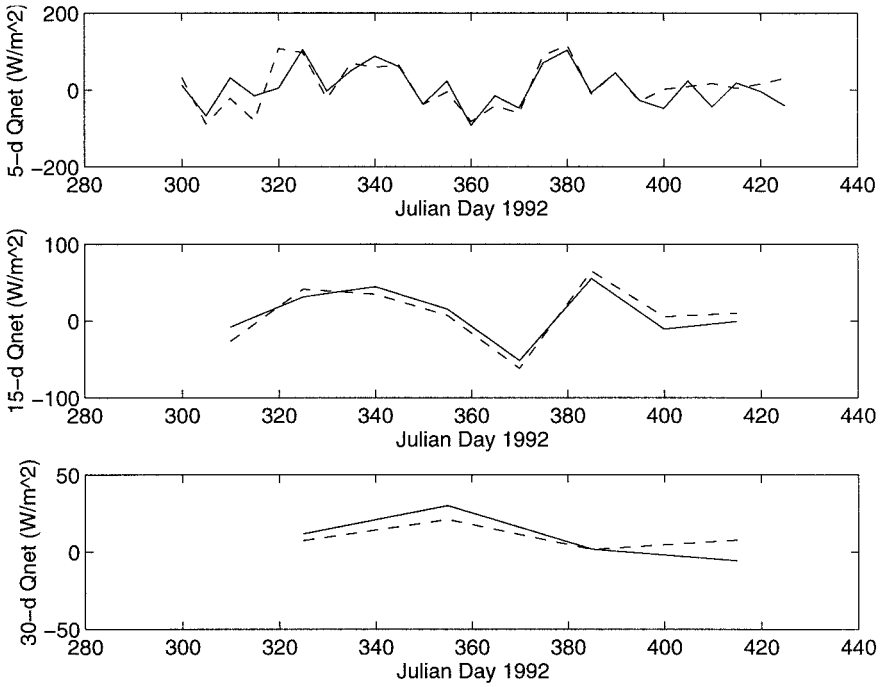

FIG. 5. Longer time-averaged net heat fluxes estimated by the bulk formula (solid) and those derived by the inverse model with observed SST as input (dashed) for the WHOI buoy. Upper: 5-day average; middle: 15-day average; lower: 30-day average.

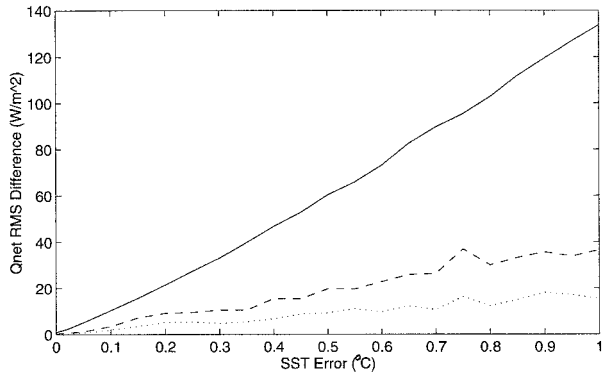

FIG. 6. Ensemble average of rms differences from 10 test runs between daily mean (solid), 15-day averaged (dashed), and 30-day averaged (dotted) net heat fluxes estimated by the bulk formula and those derived by the inverse model as a function of the amplitude of SST random error.

W m^{-2}, respectively. The rms differences of 5-day, 15-day, and 30-day averaged net heat fluxes are 36.5, 12.1, and 8.4 W m^{-2}, respectively, which are much smaller than the rms difference of 115.3 W m^{-2} recorded for the 1-day average.

The phenomenon of large variation of daily mean surface net heat flux can be explained by an experiment that shows that net heat flux is highly sensitive to relatively small SST errors in the input. Large variation of flux cannot produce very large temperature signals during a short period. For example, a 50 W m^{-2} flux variation during a period of 12 hours induces a final temperature change of only 0.1°C in a 5-m deep well-mixed layer (Gaspar et al. 1990). In our case, the mixed layer depth is greater than 5 m and hourly SST change in observed SST is sometimes as large as 0.8°C. This induces a large flux variation to balance the large SST change. The inverse model performs better for larger scales since the longer time-averaged SST has much less error and variability, which requires less variation of net heat flux to balance it. To prove this high sensitivity, some random error is added to the numerical model simulated SST when we use the bulk formula estimated net heat flux and wind stresses as forcing and then use this error-added SST as the inverse model input for the WHOI buoy data. Figure 6 shows the ensemble average of rms differences from 10 test runs between the daily mean, 15-day averaged, and 30-day averaged net heat fluxes estimated by the bulk formula and those derived by the inverse model as a function of the amplitude of SST random error. We can see that the rms difference increases almost linearly with SST error. We also prove that the longer time-averaged net heat flux estimated by the inverse model has lower rms difference from the bulk formula estimation.

The application of satellite data is tested by using the blended SST described in section 3 as the inverse model input. Figure 7 shows the comparison between the daily mean WHOI mooring measured SST and blended SST (*NOAA-11, -12* AVHRR-derived SST blended with mooring measured SST) during TOGA COARE IOP. The trend of the blended SST agrees well with the mooring measured SST. Now a reasonable diurnally varying amplitude appropriate for SST is applied to obtain hourly blended SST. The inverse model was rerun with this hourly blended SST instead of hourly mooring measured SST while observed wind stresses and rain rate remained the same. Figure 8 shows the comparison between longer time-averaged net heat fluxes estimated by the bulk formula and those derived by the inverse model with the blended SST as input for the WHOI

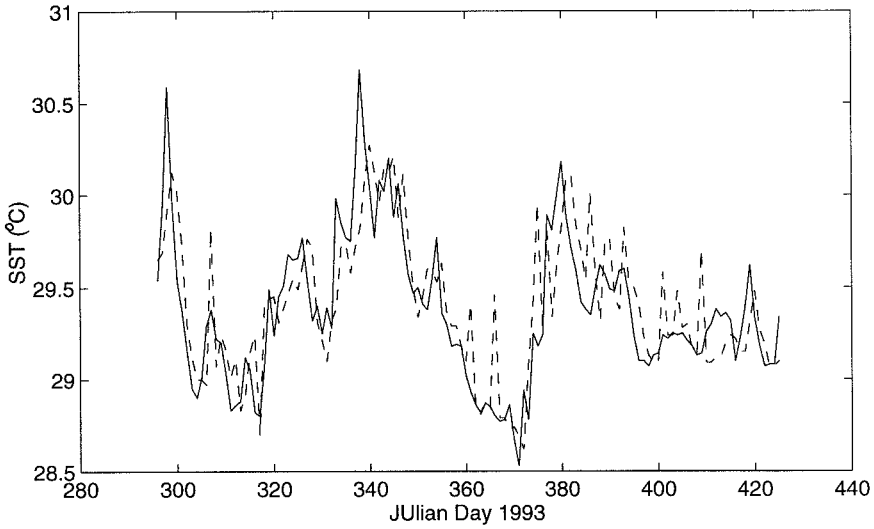

FIG. 7. Daily mean mooring measured SST (solid) and blended SST (*NOAA-11, -12* AVHRR derived SST blended with mooring measured SST) (dashed) during TOGA COARE IOP for the WHOI buoy.

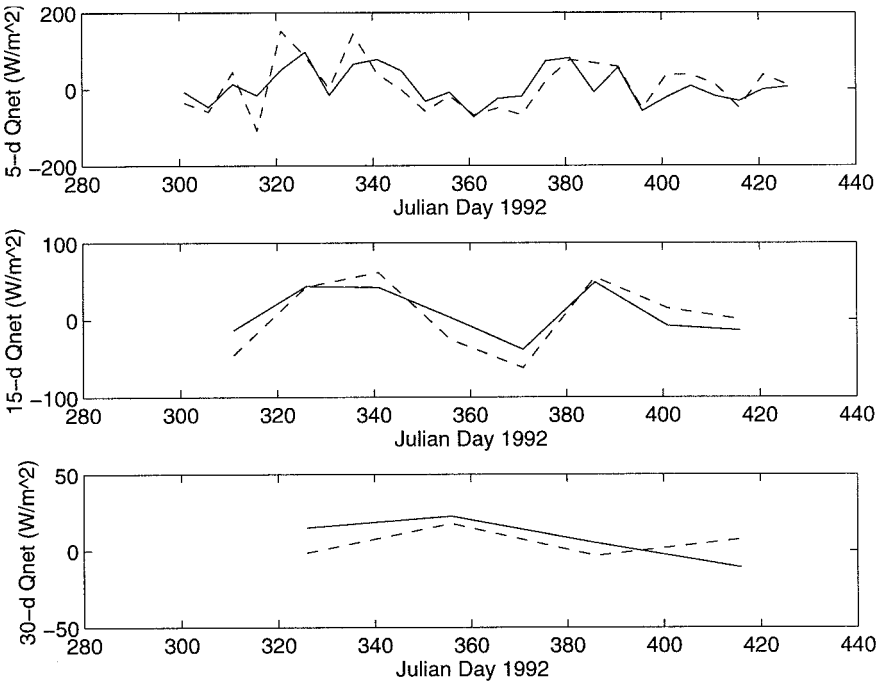

FIG. 8. Longer time-averaged net heat fluxes estimated by the bulk formula (solid) and those derived by the inverse model with the blended SST as input (dashed) for the WHOI buoy. (There is a 1-day shift in average compared to Fig. 5). Upper: 5-day average; middle: 15-day average; lower: 30-day average.

buoy. In order to validate the model independence from the starting day of average, there is a 1-day shift in Fig. 8 compared to Fig. 5. The correlation coefficients between the two lines for 5-day, 15-day, and 30-day averaged net heat fluxes are 0.73, 0.90, and 0.28, respectively. The mean differences for 5-day, 15-day, and 30-day averaged net heat fluxes are 11.45, 14.16, and 14.16 W m^{-2}, respectively. And the rms differences are 38.3, 12.8, and 9.1 W m^{-2}, respectively. The comparison with the inverse model estimations from the mooring measured SST (Fig. 5) shows that usage of the blended SST apparently decreases the correlation coefficients and increases mean differences and rms differences. This is because the blended SST has less accuracy than the mooring-measured SST at this site. Presently, the reported absolute SST accuracy from satellite observation in the tropical regions is about 0.5°C (McClain et al. 1985; Wick et al. 1992). But the rms difference of daily mean net heat flux estimation for an error of 0.5°C in hourly SST is about 60 W m^{-2} (Fig. 6). It is smaller than the 80 W m^{-2} differences sometimes shown for bulk formulas. And the rms differences for 15-day and 30-day averaged net heat fluxes for an error of 0.5°C in hourly SST are only about 20 W m^{-2} and 10 W m^{-2} (Fig. 6), which are quite acceptable. Generally speaking, satellite data has the advantage of high temporal and spatial coverage with high accuracy. The inverse model can be applied to a large domain using satellite data.

5. Summary

In this study, we have investigated the surface net heat flux in the western equatorial Pacific, a region of generally high SST and low wind speed. A one-dimensional model can be used here because of the weak horizontal advection.

We compared surface heat fluxes computed by bulk parameterization method with those computed from an inverse ocean model. A one-dimensional, level 2.5 turbulence-closure mixed layer inverse model is used to estimate surface net heat flux. The inverse model produces large variations for daily mean net heat flux estimation, while the derived longer time-averaged net heat flux is more accurate and compared better with observations. Estimated net surface heat flux is found to be highly sensitive to relatively small SST errors in the input. Satellite data can be used as input in both the bulk formula and the inverse method.

The latent and sensible heat fluxes provided by TOGA COARE, which is computed from a bulk formula that involves more parameters and processes than the LKB formula does, do not show significant difference from LKB results in our limited comparison.

Surface heat fluxes are very difficult to observe and bulk formulas have their inherent inaccuracies. An inverse model is a promising alternative to be explored. The model SST produced by a 1D model in a small horizontal advection region cannot be consistent with

the observed SST, mainly due to the inaccurate forcing heat fluxes that are usually derived from bulk formulas. The inverse model takes advantage of the accurately observed SST input to be able to reproduce the correct net heat flux. To apply the inverse approach over a larger area where the horizontal advection is not small, a vertical mixing scheme embedded in a three-dimensional general circulation model would be needed to calculate the surface heat fluxes. Such effort, though more complicated, is worth trying. The advantage is that all the model inputs (wind stresses, SST, and net shortwave radiation) can be provided by satellite measurements with adequate spatial and temporal resolutions.

Acknowledgments. We would like to thank Robert Weller and the Woods Hole Oceanographic Institution for TOGA COARE meteorological data time series. GPCP IR-based precipitation data is provided by Robert Joyce and ISCCP cloud cover is provided by Dake Chen. We also want to thank William Emery and Keith Cherkauer at University of Colorado for providing the various satellite-observed SST products during TOGA COARE IOP. We thank Sudhir Nadiga, Pablo Clemente-Colon, and Richard Field for their assistance in the modification of the manuscript. This work is supported partially by the National Science Foundation through Grant NSF-OCE/9453499 and by the Earth Observing System (EOS) Interdisciplinary Science investigation of the National Aeronautics and Space Administration. We would also like to thank the anonymous reviewers for their helpful suggestions.

REFERENCES

Bishop, J. K. B., and W. B. Rossow, 1991: Spatial and temporal variability of global surface solar irradiance. *J. Geophys. Res.*, **96,** 16 839–16 858.

Buck, A. L., 1981: New equations for computing vapor pressure and enhancement factor. *J. Appl. Meteor.,* **20,** 1527–1532.

Chen, D., and L. M. Rothstein, 1991: Modeling the surface mixed layer structure in the western equatorial Pacific. *TOGA-Notes,* **2,** 13–16.

——, A. J. Busalacchi, and L. M. Rothstein, 1994a: The roles of vertical mixing, solar radiation, and wind stress in a model simulation of the sea surface temperature seasonal cycle in the tropical Pacific Ocean. *J. Geophys. Res.,* **99** (C10), 20 345–20 359.

——, L. M. Rothstein, and A. J. Busalacchi, 1994b: A hybrid vertical mixing scheme and its application to tropical ocean models. *J. Phys. Oceanogr.,* **24,** 2156–2179.

Delcroix, T., G. Eldin, M. H. Radenac, J. Toole, and E. Firing, 1992: Variations of the western equatorial Pacific Ocean, 1986–1988. *J. Geophys. Res.*, **97,** 5423–5445.

Dillon, T. M., J. N. Moun, T. K. Chereskin, and D. R. Caldwell, 1989: Zonal momentum balance at the equator. *J. Phys. Oceanogr.*, **19,** 561–570.

Fairall, C. W., E. F. Bradley, D. P. Rogers, J. B. Edson, and G. S. Young, 1996: Bulk parameterization of air–sea fluxes for Tropical Ocean-Global Atmosphere Coupled Ocean-Atmosphere Response Experiment. *J. Geophys. Res.,* **101** (C2), 3747–3764.

Gaspar, P. H., J.-C. André, and J.-M. Lefevre, 1990: The determination of the latent and sensible heat fluxes at the sea surface viewed as an inverse problem. *J. Geophys. Res.,* **95** (C9), 16 169–16 178.

Gautier, C., and R. Frouin, 1985: Satellite-derived ocean surface radiation fluxes. *Advances in Remote Sensing Retrieval Methods,* H. E. Fleming and M. T. Chahine, Eds., A. Deepak, 311–329.

——, G. Diak, and S. Masse, 1980: A simple physical model to estimate incident solar radiation at the surface from GOES satellite data. *J. Appl. Meteor.,* **19,** 1005–1012.

Giese, B. S., and D. R. Cayan, 1993: Surface heat flux parameterization and tropical Pacific sea surface temperature simulations. *J. Geophys. Res.,* **98** (C4), 6979–6989.

Godfrey, J. S., and E. J. Lindstrom, 1989: The heat budget of the equatorial western Pacific surface mixed layer. *J. Geophys. Res.,* **94,** 8007–8017.

Goff, J. A., and S. Gratch, 1946: Low-pressure properties of water from −160° to 210°F. *Trans. Amer. Soc. Heat. Vent. Eng.,* **52,** 95–121.

Janowiak, J. E., and P. A. Arkin, 1991: Rainfall variations in the tropics during 1986–1989, as estimated from observations of cloud-top temperature. *J. Geophys. Res.,* **96** (Suppl), 3359–3373.

Large, W. G., and S. Pond, 1982: Sensible and latent heat flux measurements over the ocean. *J. Phys. Oceanogr.,* **12,** 464–482.

Liu, W. T., 1984: Estimation of latent heat flux with SEASAT-SMMR, a case study in north Atlantic. *Large-Scale Oceanographic Experiments and Satellites,* C. Gautier and M. Fieux, Eds., D. Reidel, 205–221.

——, 1988: Moisture and latent heat flux variabilities in the tropical Pacific derived from satellite data. *J. Geophys. Res.,* **93** (C6), 6749–6760.

——, 1990: Remote sensing of surface turbulence heat flux. *Surface Waves and Fluxes,* G. C. Geernaert and W. J. Plant, Eds., Vol. II, Kluwer Academic, 293–309.

——, 1993: Evaporation from the ocean. *Global Change Atlas,* R. Gurney, J. Foster, and C. Parkinson, Eds., Cambridge University Press, 265–278.

——, and P. P. Niiler, 1984: Determination of monthly mean humidity in the atmospheric surface layer over oceans from satellite data. *J. Phys. Oceanogr.,* **14,** 1451–1457.

——, and C. Gautier, 1990: Thermal forcing on the tropical Pacific from satellite data. *J. Geophys. Res.,* **95** (C8), 13 209–13 217.

——, K. B. Katsaros, and J. A. Businger, 1979: Bulk parameterization of air–sea exchanges of heat and water vapor including the molecular constraints at the interface. *J. Atmos. Sci.,* **36,** 1722–1735.

——, W. Tang, and R. Atlas, 1993: Sea surface temperature exhibited by an ocean general circulation model in response to the wind forcing derived from satellite data. *Satellite Remote Sensing of the Oceanic Environment,* S. F. Jones, Y. Sugimori, and R. W. Stewart, Eds., Seibutsu Kenkyusha, 350–355.

——, A. Zhang, and J. K. B. Bishop, 1994: Evaporation and solar irradiance as regulators of the seasonal and interannual variabilities of sea surface temperature. *J. Geophys. Res.,* **99,** 12 623–12 637.

——, W. Tang, and L. L. Fu, 1995: Recent warming event in the Pacific may or may not be an El Niño. *Eos, Trans. Amer. Geophys. Union,* **76,** 429–437.

Lowe, P. R., 1977: An approximating polynomial for the computation of saturation vapor pressure. *J. Appl. Meteor.,* **16,** 100–103.

Lukas, R., and E. Lindstrom, 1991: The mixed layer of the western equatorial Pacific Ocean. *J. Geophys. Res.,* **96** (Suppl), 3343–3357.

Lumb, F. E., 1964: The influence of cloud on hourly amount of total solar radiation at the sea surface. *Quart. J. Roy. Meteor. Soc.,* **90,** 43–56.

McClain, E. P., W. G. Pichel, and C. C. Walton, 1985: Comparative performance of AVHRR-based multichannel sea surface temperatures. *J. Geophys. Res.,* **90** (C6), 11 587–11 601.

Mellor, G. L., and T. Yamada, 1982: Development of a turbulence closure model for geophysical fluid problems. *Rev. Geophys. Space Phys.,* **20,** 851–875.

Miller, J. R., 1981: Variations in upper ocean heat storage determined from satellite data. *Remote Sens. Environ.,* **11,** 473–482.

Paulson, C. A., and J. J. Simpson, 1977: Irradiance measurements in the upper ocean. *J. Phys. Oceanogr.,* **7,** 952–956.
Reed, R. K., 1977: On estimating insolation over the ocean. *J. Phys. Oceanogr.,* **7,** 482–485.
Rossow, W. B., and R. A. Schiffer, 1991: ISCCP cloud data products. *Bull. Amer. Meteor. Soc.,* **72,** 2–20.
Sargent, G. P., 1980: Computation of vapor pressure, dew point and relative humidity from dry- and wet-bulb temperatures. *Meteor. Mag.,* **109,** 238–246.
Seager, R., S. E. Zebiak, and M. A. Cane, 1988: A model of the tropical Pacific sea surface temperature climatology. *J. Geophys. Res.,* **93** (C2), 1265–1280.
Smith, S. D., 1988: Coefficients for sea surface wind stress, heat flux, and wind profiles as a function of wind speed and temperature. *J. Geophys. Res.,* **93** (C12), 15 467–15 472.
Sprintall, J., and M. J. McPhaden, 1994: Surface layer variations observed in multiyear time series measurements from the western equatorial Pacific. *J. Geophys. Res.,* **99** (C1), 963–979.
Stevenson, J. W., and P. P. Niiler, 1983: Upper ocean heat budget during the Hawaii-to-Tahiti shuttle experiment. *J. Phys. Oceanogr.,* **13,** 1894–1907.
Talley, L. D., 1984: Meridional heat transport in the Pacific Ocean. *J. Phys. Oceanogr.,* **14,** 231–241.
Weare, B. C., 1989: Uncertainties in estimates of surface heat fluxes derived from marine reports over the tropical and subtropical oceans. *Tellus,* **41A,** 357–370.
Weller, R. A., and S. P. Anderson, 1996: Surface meteorology and air–sea fluxes in the western equatorial Pacific warm pool during the TOGA Coupled Ocean–Atmosphere Response Experiment. *J. Climate,* **9,** 1959–1990.
Wick, G. A., W. J. Emery, and P. Schluessel, 1992: A comprehensive comparison between satellite-measured skin and multichannel sea surface temperature. *J. Geophys. Res.,* **97** (C4), 5569–5595.
Yan, X.-H., and A. Okubo, 1992: Three-dimensional analytical model for the mixed layer depth. *J. Geophys. Res.,* **97** (C12), 20 201–20 226.
——, C.-R. Ho, Q. Zheng, and V. Klemas, 1992: Temperature and size variabilities of the western Pacific warm pool. *Science,* **258,** 1643–1645.
——, Y. He, W. T. Liu, Q. Zheng, and C.-R. Ho, 1997: Centroid motion of the western Pacific warm pool in the three recent El Niño–Southern Oscillation events. *J. Phys. Oceanogr.,* **27,** 837–845.